IAC–22–C1.IPB.39.x71903

GNC of a cargo spacecraft for on-orbit servicing of Herschel at L₂

Andrea Siena
Graduate student at Politecnico di Torino, Italy, andreasiena97@gmail.com

Ahmed Mahfouz
University of Luxembourg, Luxembourg, Ahmed.mahfouz@uni.lu

Davide Menzio
University of Luxembourg, Luxembourg, Davide.menzio@uni.lu

Holger Voos
University of Luxembourg, Luxembourg, Holger.voos@uni.lu

Thomas Passvogel
Formerly European Space Agency (ESA), The Netherlands, thomas.passvogel@online.de

Abstract
It is anticipated that space exploration will need to rely on In Situ Resource Utilization (ISRU) in order to extend spacecraft lifetime and/or reduce the missions cost and/or the cruise time. For the Moon and, in the future, Mars colonization, relying on in-situ resources is a necessary step to become independent from the Earth. The possibility to produce resources on the Moon is advantageous for those missions that are too far from the Earth to be resupplied. At the SnT Research Centre, the Luxembourg Space Agency is supporting a feasibility study to assess the benefit of on-orbit servicing (OOS), exploiting lunar resources for the Herschel Space Observatory. Herschel ended its operations in 2013 as a consequence of the depletion of its coolant and, in turn, of the capability of cooling down its instruments. To extend its operations, a resupply mission has been envisaged relying on an adapted cargo spacecraft employed in lunar gateway operations. This paper deals with the trajectory design and optimization of the cargo on its journey from the Moon to rendezvous with Herschel and with orbit and attitude control. Considering Herschel's orientation on its orbit, with the sunshield in the direction of the Sun and the need to access to Herschel's rear panel to perform the resupply operation, a final approach along the negative x-axis, where the primaries lie, is considered. A multiple shooting technique is used to perform a flanking manoeuvre. Moreover, an attitude control algorithm is adopted to track the attitude trajectory provided by the guidance algorithms which, in turn, ensure minimum thrusting errors of the cargo spacecraft and a continuous visibility of Herschel. In future works, different perturbations will be considered and angular rates induced by the movement of the robotic arms will be compensated.

keywords: Herschel, L₂, rendezvous, optimization, close proximity operations, attitude control

1. Introduction

The study was conducted as master's thesis [1] in collaboration with the University of Luxembourg as part of its project to assess the feasibility of a mission to refill the coolant of the Herschel Space Observatory. In order to accomplish the mission, a cargo spacecraft will be launched from the Moon and will set up on an interplanetary trajectory towards the Sun-Earth L₂ (SEL_2) point to finally rendezvous with Herschel and start the docking operations. During the final approach phase, the attitude of the s/c will be controlled to respect the constraints of the mission.

Rendezvous and docking operations have been the focus of many missions in the last years. The first successful one was the GEMINI mission [2], accomplished in 1966. From that day on, more and more missions involved RdV between two or more s/c for different reasons, such as bringing supplies or crew members to an existing station, debris removal or performing on - orbit activities like refueling, repairing or assembling of new structures.

The Orbital Express programme [3] developed by the National Aeronautics and Space Administration *(NASA)* had the goal of demonstrating and validating key technologies just for these purposes. It con-

sisted of two spacecrafts performing rendezvous and capture in order to replace batteries or refueling propellant. However, the outcome of the mission remained confidential, making it difficult to assess what has been achieved, but another mission, called Proba - 3 [4], carried out by the European Space Agency *(ESA)*, presents more insights on the topic. The mission aimed at improving formation flying technologies performing solar coronography and formation manoeuvre demonstrations between two s/c that would be inserted in a high elliptical orbit as a single rigid body and then separated. Then, formation flying operations would begin with the acquisition of the relative state in terms of position, velocity and attitude. The simulation results demonstrated the possibility of achieving a two year mission with a ΔV around 10 m/s for the main operations and a ΔV between 100 and 250 mm/s for station - keeping *(SK)* manoeuvres.

In the field of orbital rendezvous, many information can also be found in Gaias and D'Amico's works. They carried out several demonstrations in Low Earth Orbit *(LEO)* to validate autonomous systems based on angles - only measurements to perform far - to mid - range distance RdV activities to a non - cooperative target. ARGON [5] and AVANTI [6, 7, 8] have been conducted during the extended phases of the PRISMA mission for this purpose, obtaining remarkable results. The first demonstration performed an efficient and safe RdV from 30 km to a final hold point of 3 km from the target. The second experiment differed from the latter by its complexity since no target tracking data were available and the orbit was lower than ARGON's one, leading to a stronger drag perturbation and the presence of eclipses.

All these missions rely on Guidance, Navigation & Control *(GNC)* algorithms and Optical Navigation *(ON)* techniques to be fully automated and allow a more flexible manoeuvre design. Rebordão [9] presented an overall description of ON modes and methods in his work. The main idea is to use objects with reliable ephemerides as beacons, enabling the navigation subsystem to locate the s/c in space and plan subsequent manoeuvres to accomplish a mission. The camera provides line of sight *(LoS)* estimates to the GNC system, which combines them with the output of other sensors to generate the best possible estimation of the state of the s/c. In this perspective, Llop [10] defined an effective GNC system for Earth - Moon *(EM)* libration point missions that reduced operational and ground infrastructure costs. He started with optical measurements of the Moon to perform

the state estimation and then used a Target Point control technique to compute correction manoeuvres. Trajectory design in three - body systems has been assessed from many points of view. Due to their uniqueness, in fact, Lagrangian (or libration) points became the focus of many missions, most of the which accomplished in order to settle space telescopes or other observatories like Herschel in a region of space where the equilibrium of forces would allow a reduction of disturbances. Folta [11], for example, used a dynamical system approach to get reference solutions in the multi - body problem for Sun-Earth *(SE)* libration orbits and then used the associated stable and unstable manifolds to generate transfer trajectories towards them. He also found different optimized strategies assessing ΔV and time for both high and low thrust manoeuvres. Similarly, Thepdawala [12] optimized transfer trajectories in the EM system using differential evolution suited for an early stage speedy mission design process. Both EM and SE systems though, require manoeuvres with high ΔV cost and short optimal spacing. Moreover, adding constraints like performing a RdV manoeuvre, lowers the number of possible transfers and forces the timing to be planned well in advance [13].

After a swift introduction of the problem and the literature found to support the studies, an overview of the Lunar infrastructure and the environment in which the cargo will operate is presented in section 2. Following, in section 3, the methodology used for the trajectory design is presented and successively the linearization process is described in section 4. Section 5 deals with the close proximity operations presenting the method used for the rendezvous phase. Section 6 features the assumptions made for a first assessment of an attitude control technique of the spacecraft during the rendezvous phase. In the end, section 7, draws the conclusions on the results obtained and presents the future iterations of the mission.

2. Background

2.1 *Circular Restricted 3 - Body Problem*

In the most general case, a body in space undergoes many different forces: gravitational pull, drag, solar pressure, magnetic forces. These forces may vary according to the position of the body and affect its motion, so they must be taken into account to study the evolution of its trajectory, especially if accurate operations have to be carried out.

For the Herschel Re-Supply Mission *(HRSM)*, the cargo s/c will be travelling between the Moon and the SEL_2 point, thus the main disturbances will be

constituted by the Sun, the Earth and the Moon's gravitational pull, whereas the attraction of all the other bodies of the Solar System can be neglected [14]. Furthermore, if the effects of the Moon are included in those of the Earth, the two can be accounted as a single body, obtaining the so called 3 - Body Problem *(3BP)* [14]. Considering only the main bodies allows easier calculations that would be too computationally expensive in the most general case and would add unnecessary complexity to the problem. The first main body would be the Sun (m_1), the second the system composed of the Earth and the Moon (m_2) and the third would be the spacecraft (m). Moreover, assuming that $m_1 > m_2 >> m$, the problem addressed becomes the Restricted 3 - Body Problem *(R3BP)*, where the mass of the s/c is neglected. Another simplification is made considering the Earth's orbit as almost circular ($e = 0.0167$) meaning that the eccentricity can be considered null and added at a later time to test its impact on the dynamics. The R3BP becomes the Circular Restricted 3 - Body Problem *(CR3BP)*. Moreover, the equations of motion are usually expressed in a rotating frame, called synodic, centered on the barycenter of the system and rotating with the angular rate of the second primary. Figure 1 shows the two frames, inertial and synodic, and the three bodies involved. The total mass can be defined as $M = m_1 + m_2$ and used to normalize the single masses. By doing so the parameter $\mu = m_2/M$ is defined, so that the barycenter of the 3 - body system has coordinates $B = [\mu R \; 0 \; 0]^{\mathrm{T}}$ w.r.t. the inertial system placed on the main primary, where R is the distance between the two primaries. Accordingly, the coordinates of the three bodies in the synodic frame will be the following:

$$
m_1 = \begin{Bmatrix} -\mu R \\ 0 \\ 0 \end{Bmatrix} \quad m_2 = \begin{Bmatrix} R(1-\mu) \\ 0 \\ 0 \end{Bmatrix} \quad m = \begin{Bmatrix} x \\ y \\ z \end{Bmatrix} \quad (1)
$$

The normalization helps expressing the equations in such a way that they are dependent only on one parameter, μ. Therefore the other variables are also normalized, the time relative to the mean motion of the system $\omega = \sqrt{\frac{GM}{R^3}}$, with $G = 6.67 \cdot 10^{-11} \frac{Nm^2}{Kg^2}$ being the gravitational constant, and the distances relative to R. By doing so, the dimensionless non - linear equations of motion are obtained [14]:
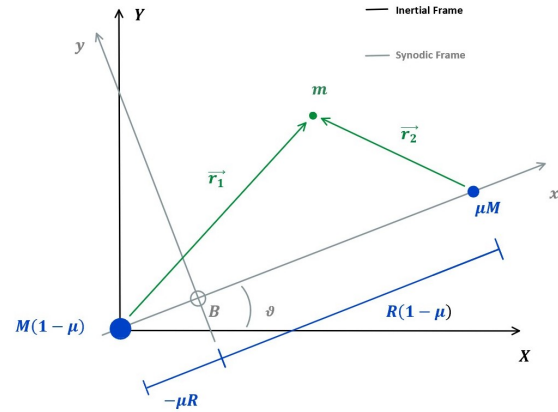

Fig. 1: Restricted Three - Body Problem

$$
\ddot{x} = 2\dot{y} + x - \frac{(1-\mu)(x+\mu)}{r_1^3} - \frac{\mu(x-1+\mu)}{r_2^3}
$$

$$
\ddot{y} = -2\dot{x} + y - \frac{(1-\mu)y}{r_1^3} - \frac{\mu y}{r_2^3} \qquad (2)
$$

$$
\ddot{z} = -\frac{(1-\mu)z}{r_1^3} - \frac{\mu z}{r_2^3}
$$

with r_1 and r_2 being the distances of the s/c respectively from the first and the second primary such that

$$
r_1 = \sqrt{(x+\mu)^2 + y^2 + z^2}
$$
$$
r_2 = \sqrt{(x-1+\mu)^2 + y^2 + z^2} \qquad (3)
$$

2.2 *The ESA mission*

HERSCHEL [15] is a space observatory dedicated to collecting measurements in the far - infrared band of the spectrum. Its main goal is to study the chemical composition of planetary systems, observe the birth of new galaxies and stars and follow their evolution. Herschel was launched on 14 May 2009 from Kourou space centre by an Arian V ECA launcher, shared with another telescope, PLANCK. It was put in a 800000 km Lissajous orbit around Sun-Earth L_2, beyond the Earth-Moon system, far away from heat and light emissions of our planet, performing every month SK manoeuvres of not more than 1 m/s per year to maintain the orbit due to its instability. The nominal orbit was chosen among a manifold of different orbits such that its stable manifold touched the best Ariane launch conditions [16]. The mission lifetime was determined by the predicted cryostat service life of 3.5 years.

Herschel has a modular design [17] consisting of the payload module *(PLM)* supporting the telescope, the sunshade/sunshield and the service module *(SVM)*. The PLM is dominated by the cryostat vacuum vessel *(CVV)* from which the helium tank is suspended, surrounded by three vapour - cooled shields to minimise parasitic heat loads. The optical bench with the three instrument focal plane units (FPUs) is supported on top of the tank. A phase separator allows a continuous evaporation of the liquid into cold gas. The FPUs and their detectors are kept at their required temperatures by thermal connections to the liquid cryogen in the tank and to pick - off points at different temperatures of the piping that carries the helium gas from the tank, which is routed around the instruments for this purpose, and to the vapour - cooled shields for eventual release into free space. The SVM houses "warm" payload electronics on four of its eight panels and provides the necessary infrastructure for the satellite such as power, attitude and orbit control, the on-board data handling and command execution, communications, and safety monitoring. It also provides a thermally controlled environment, which is critical for some of the instrument units. Finally, the SVM also provides mechanical support for the PLM, the sunshield/sunshade, a thermal shield to thermally decouple the PLM from the SVM, and it ensures the main mechanical load path during the launch. Figure 2 shows, on the left, the payload module with all the components mentioned above, in the middle, a close-up image on the payload module itself displaying the optical bench for the FPUs on top of the helium tank and the focal plane cover with the vapour-cooled shields inside the CVV and finally, on the right, the telescope being prepared for acoustic testing in the Large European Acoustic Facility *(LEAF)* in the European Space and Technology Test Centre.
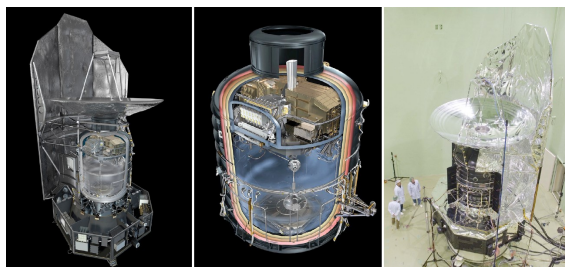
Wet mass (helium)	3400 (335) kg
Dry mass	2800 kg
Height	7.5 m
Cross section	4×4 m
Wavelength	$[55 \div 672]$ μm
Telescope	Cassegrain
Mirrors	3.5 m primary 0.3 m secondary

Table 1: Platform

Fig. 2: *Left:* Herschel with PLM, cryostat, FPUs, telescope, and SVM. *Middle:* close-up of the PLM. *Right:* Preparation for acoustic testing

Table 1 provides the physical features of the observatory.

The Herschel resupply mission was envisaged to put the Space Observatory *(SO)* back on line, refueling the cryostat with the coolant extracted on the Moon. In order to do so, the (^{4}He) will be extracted from the regolith and filled into a supply cryostat in an adapted cargo s/c. The latter will then leave the Moon and embark on an interplanetary trajectory towards SEL_2 until it is close enough to start the Close Proximity Operation *(CPO)* phase, including rendezvous and final approach. During these phases attitude control will assure that the cargo spacecraft would be oriented in compliance with the constraints of the mission. At the end of the docking phase, when the two vehicles are connected, the refueling starts. During this operation, the new system will be controlled so that Herschel would remain on its orbit after the refueling is completed. The end of the mission foresees a safe receding phase of the cargo s/c and its return on the Moon, to be reloaded of coolant and prepared to depart again when another refueling of the observatory is needed.

The constraints to ensure the feasibility of this mission are:

- Approaching Herschel from the rear side, where the docking port is located, since the front is covered by the sunshield protecting the structure from the heat of the sun rays;

- Not crossing of the orbits for safety reasons;

- Maximum a month of journey to reach Herschel.

3. Trajectory Design

The ephemerides of the celestial bodies involved and Herschel are taken from SPICE kernels in the Sun inertial frame and are normalized relative to the average values of the astronomical distance

$l = 1.4964 \cdot 10^8$ km for the positions, to the EM circular velocity $V_c = 29.7834$ km/s for the velocities and to the EM angular rate n = $1.9907 \cdot 10^{-7}$ rad/s for the times, over a year. Finally, the ephemeris are rotated into the synodic frame, as shown in figure 3.
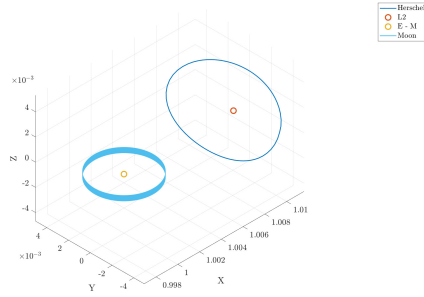

Fig. 3: Earth - Moon barycenter, Herschel, L_2, Moon in the synodic reference frame

After setting the working environment a grid search is performed to find a family of feasible trajectories to go from the Moon to Herschel. The procedure applied foresees a backward propagation from each point of the Lissajous orbit perturbing Herschel's velocity adding a ΔV to the velocity itself as expressed in the equation below:

$$\boldsymbol{v} := \boldsymbol{v} + \Delta V \cdot \hat{\boldsymbol{v}} \tag{4}$$

where ΔV is a velocity magnitude, normalized relative to V_c and added to Herschel's velocity in order to perturb its state, and $\hat{\boldsymbol{v}}$ is the velocity unit vector.

The maximum propagation time is set to - 30 days, where the negative sign serves to backward propagate. Nevertheless, it is possible that some trajectories reach the Moon before, therefore, in order to avoid passing it, an event function has been created to stop the propagation once the trajectories hit the Moon's orbit. The latter is shaped as a cylinder with axis passing through the Earth-Moon barycenter, since the Moon spans the equivalent of a hollow cylinder around the Earth because of the inclination of its orbit.

For every point of the Lissajous orbit, 20 ΔV trials are given, between -1 km/s and 1 km/s, rotating $\hat{\boldsymbol{v}}$ of seven angles around the three axes of the reference frame in which the coordinates are expressed. The angles range from 45° to 315° with a step of 45°. For those conditions that allowed reaching the Moon an extended grid search has been carried out to find the minimum velocity to establish the trajectory, decreasing the angle step to 10° and the velocity step

to 100 m/s. At least one trajectory ending up on the Moon was found for almost every starting point considered, as shown in figure 4. Figure 5 highlights the properties of the transfers found in terms of ΔV, time of flight and angle of departure from the Lissajous orbit: most of the trajectories departing from the upper side, with $0° < \theta < 180°$, are those requiring a bigger impulse to reach the Moon and, as a consequence, require less days. On the other side, most of those leaving from the lower side of the orbit, with $180° < \theta < 360°$, require half of the impulse and need more time.
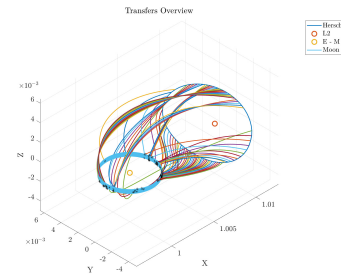

Fig. 4: Overview of the transfers found reaching the Moon. One for each considered departing point of the orbit
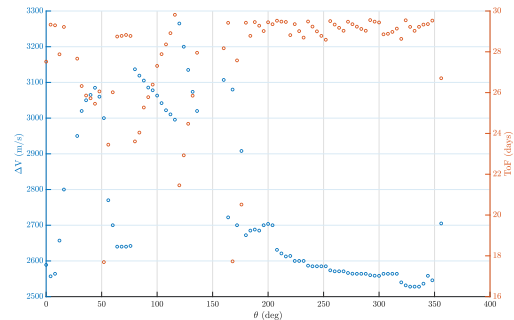

Fig. 5: Summary of ΔV and time of flight of each transfer w.r.t. the angular position of the starting point on the Lissajous orbit

4. Linearization

Linearizing the equations (2) allows a faster computation of the solution at each step solving a simple linear problem. Undoubtedly this method is worth applying only if the error due to the approximation is not too big.

Two different simplifications have been introduced:

- Linearization via Taylor series expansion;

- Hill dynamics.

A Taylor expansion at the first order needs a linearization point (x_0, y_0, z_0) and the computation of the first derivatives. After these elements have been computed and substituted in the original equations the linearized equations of motion for the 3-body dynamics are obtained:

$$\ddot{\delta x} = \underbrace{\left[1 + \frac{3(x_0 + \mu)^2 (1 - \mu) \bar{r_2}^5 + 3(x_0 - 1 + \mu)^2 \mu \bar{r_1}^5}{\bar{r_1}^5 \bar{r_2}^5}\right.}_{A_{\dot{x}x}} +$$
$$\underbrace{\left. - (1 - \mu)\bar{f_1} - \mu \bar{f_2}\right]}_{A_{\dot{x}x}} \cdot \delta x +$$
$$+ 3 y_0 \underbrace{\frac{(x_0 + \mu)(1 - \mu)\bar{r_2}^5 + (x_0 - 1 + \mu)\mu \bar{r_1}^5}{\bar{r_1}^5 \bar{r_2}^5}}_{A_{\dot{x}y}} \cdot \delta y +$$
$$+ \underbrace{2}_{A_{\dot{x}\dot{y}}} \cdot \dot{\delta y} + + 3 z_0 \underbrace{\frac{(x_0 + \mu)(1 - \mu)\bar{r_2}^5 + (x_0 - 1 + \mu)\mu \bar{r_1}^5}{\bar{r_1}^5 \bar{r_2}^5}}_{A_{\dot{x}z}} \cdot \delta z$$

$$\ddot{\delta y} = 3 y_0 \underbrace{\frac{(x_0 + \mu)(1 - \mu)\bar{r_2}^5 + (x_0 - 1 + \mu)\mu \bar{r_1}^5}{\bar{r_1}^5 \bar{r_2}^5}}_{A_{\dot{y}x}} \cdot \delta x +$$
$$- \underbrace{2}_{A_{\dot{y}\dot{x}}} \cdot \dot{\delta x} + \underbrace{\left[1 + 3 y_0^2 \frac{(1 - \mu) r_2^5 + \mu \bar{r_1}^5}{\bar{r_1}^5 \bar{r_2}^5} - (1 - \mu)\bar{f_1} - \mu \bar{f_2}\right]}_{A_{\dot{y}y}} \cdot \delta y +$$
$$+ 3 y_0 z_0 \underbrace{\frac{(1 - \mu)\bar{r_2}^5 + \mu \bar{r_1}^5}{\bar{r_1}^5 \bar{r_2}^5}}_{A_{\dot{y}z}} \cdot \delta z \quad (5)$$

$$\ddot{\delta z} = 3 z_0 \underbrace{\frac{(x_0 + \mu)(1 - \mu)\bar{r_2}^5 + (x_0 - 1 + \mu)\mu\bar{r_1}^5}{\bar{r_1}^5 \bar{r_2}^5}}_{A_{\dot{z}x}} \cdot \delta x +$$
$$+ 3 y_0 z_0 \underbrace{\frac{(1 - \mu)\bar{r_2}^5 + \mu \bar{r_1}^5}{\bar{r_1}^5 \bar{r_2}^5}}_{A_{\dot{z}y}} \cdot \delta y +$$
$$+ \underbrace{\left[3 z_0^2 \frac{(1 - \mu)\bar{r_2}^5 + \mu \bar{r_1}^5}{\bar{r_1}^5 \bar{r_2}^5} - (1 - \mu)\bar{f_1} - \mu \bar{f_2}\right]}_{A_{\dot{z}z}} \cdot \delta z$$

The linearized system (5) can be rewritten as:

$$\begin{bmatrix} \dot{\delta x} \\ \dot{\delta y} \\ \dot{\delta z} \\ \ddot{\delta x} \\ \ddot{\delta y} \\ \ddot{\delta z} \end{bmatrix} = \begin{bmatrix} 0 & 0 & 0 & 1 & 0 & 0 \\ 0 & 0 & 0 & 0 & 1 & 0 \\ 0 & 0 & 0 & 0 & 0 & 1 \\ A_{\dot{x}x} & A_{\dot{x}y} & A_{\dot{x}z} & 0 & 2 & 0 \\ A_{\dot{y}x} & A_{\dot{y}y} & A_{\dot{y}z} & -2 & 0 & 0 \\ A_{\dot{z}x} & A_{\dot{z}y} & A_{\dot{z}z} & 0 & 0 & 0 \end{bmatrix} \begin{bmatrix} \delta x \\ \delta y \\ \delta z \\ \dot{\delta x} \\ \dot{\delta y} \\ \dot{\delta z} \end{bmatrix} \quad (6)$$

where $A_{\dot{x}x}, A_{\dot{x}y}, A_{\dot{x}z}, A_{\dot{y}x}, A_{\dot{y}y}, A_{\dot{y}z}, A_{\dot{z}x}, A_{\dot{z}y},$ and $A_{\dot{z}z}$ can be easily drawn from (5). In the sequel, the Jacobian matrix of this system is referred to as $\mathbf{A}$.

The Hill problem is valid in case two of the three masses of a 3-body problem are small when compared to the other and in case these two masses are close to each other relative to their distance from the third. In the HRSM the cargo s/c is moving under the perturbations of the Earth-Moon binary system, considered as a single body, and the Sun. The latter is much bigger than the first two bodies and it is further away from Herschel than the EM system and the cargo. To quantify, the Hill approximation is accurate as long as the distance between the two smaller masses is within $\mu^{1/3} \approx 0.0145$. The distance between the EM barycenter and the further point reached by Herschel around its orbit is 0.0112, thus acceptable results are expected.

Hill equations of motion are expressed as follows:

$$\begin{cases} \ddot{x} = 2\dot{y} + (3 - \frac{1}{r^3})x \\ \ddot{y} = -2\dot{x} - \frac{y}{r^3} \\ \ddot{z} = -(1 + \frac{1}{r^3})z \end{cases} \quad (7)$$

Again, the system can be linearized and the Jacobian matrix of the system can be built.

$$\boldsymbol{A} = \begin{bmatrix} 0 & 0 & 0 & 1 & 0 & 0 \\ 0 & 0 & 0 & 0 & 1 & 0 \\ 0 & 0 & 0 & 0 & 0 & 1 \\ 3 - \frac{1}{r^3} & 0 & 0 & 0 & 2 & 0 \\ 0 & -\frac{1}{r^3} & 0 & -2 & 0 & 0 \\ 0 & 0 & -(1 + \frac{1}{r^3}) & 0 & 0 & 0 \end{bmatrix}$$

where $r = \sqrt{x^2 + y^2 + z^2}$.

4.1 *Simulations - Close Proximity Operations*

The linear system can be solved using the following equation

$$\boldsymbol{x}(t_{k+1}) = \boldsymbol{\Phi}(t_k, \ t_{k+1}) \cdot \boldsymbol{x}(t_k) \quad (8)$$

where t_{k+1} is the time step successive to t_k. $\boldsymbol{\Phi}$ is the state transition matrix *(STM)* and it can be computed in two different ways:

1. $\boldsymbol{\Phi}_1 = \mathbb{1}_{6 \times 6} + \boldsymbol{A} \cdot \Delta t$

2. $\boldsymbol{\Phi}_2 = e^{\boldsymbol{A} \cdot \Delta t}$

In both cases the variable $\Delta t := t_{k+1} - t_k$ is negative to perform a backward propagation.

In order to assess the efficiency and fastness of the linear resolution of the equations of motion, the linearized dynamics is also propagated through `ode45` and the results compared in term of accuracy and computational time.

Therefore, in order to decide which approximation works best, the different equations are tested on the last 5 km of one of the trajectories found: the requiring the minimum amount of ΔV.

By looking at figure 6, it is clear that the propagation with $\boldsymbol{\Phi}_1$ performs better for the position error, whereas there are very little differences for the velocity. The results obtained with $\boldsymbol{\Phi}_2$, on the other hand, are comparable to the use of the `ode45` function for efficiency. Moreover, the linear system solved with $\boldsymbol{\Phi}_1$ is about three times faster than the one solved using $\boldsymbol{\Phi}_2$, while the propagation with the Runge-Kutta method is 1000 times slower than using any of the state transition matrices.
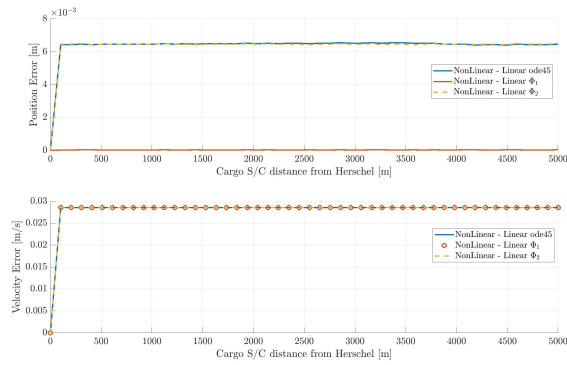

Fig. 6: Position and velocity errors for the CPO trajectory propagated with the linear dynamics obtained via Taylor series expansion

The same logic is used for the Hill dynamics, obtaining the results in figure 7. They point out that, in this case as well, the use of $\boldsymbol{\Phi}_1$ is the best for what concerns the position, but unlike in the Taylor approximation, $\boldsymbol{\Phi}_2$ performs worse than the other two. Furthermore, the propagation with `ode45` performs better for what regards the velocity. As well as for the Taylor approximation, the linear resolution with $\boldsymbol{\Phi}_1$ is the fastest, followed by the resolution with $\boldsymbol{\Phi}_2$ and then by the propagation with `ode45`.

The propagation with the $\boldsymbol{\Phi}_1$ is preferred over $\boldsymbol{\Phi}_2$ and `ode45` because it brings to better results in velocity for the Hill approximation and turns out to be faster.

Eventually, the two linearization procedures, propagated with $\boldsymbol{\Phi}_1$, are compared and, in figure 8, it can be seen that the Hill approximation performs slightly
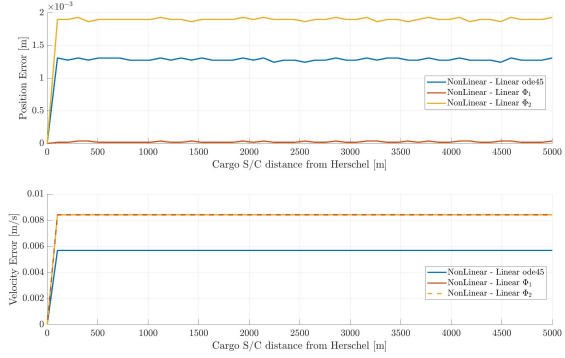

Fig. 7: Position and velocity errors for the CPO trajectory propagated with the Hill's dynamics
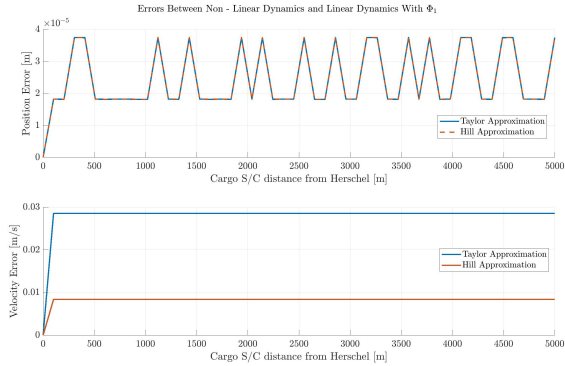

Fig. 8: Comparison between Taylor and Hill's approximations for position and velocity in CPO

better in velocity while giving the same errors in position.

In conclusion, the state propagation with a linear system resolution using the Hill dynamics and the STM $\boldsymbol{\Phi}_1$ results being better, therefore it will be used as a linearization technique in the rendezvous phase together with the non-linear dynamics.

5. Rendezvous

In order to be compliant with the regulations, the common parameters of the International Rendezvous System Interoperability Standards *(IRSIS)* have been adopted, initiating RdV at 5 km from Herschel and starting the approach from outside the Keep-Out-Sphere KOS. Moreover, the approach has to be performed with a low relative velocity w.r.t. the target in order to actuate abortion manoeuvres in case one of the systems doesn't work as expected or the approach cannot be performed in a safe way for other reasons. In addition, for the HRSM, the approach corridor can be expanded thanks to the possibility
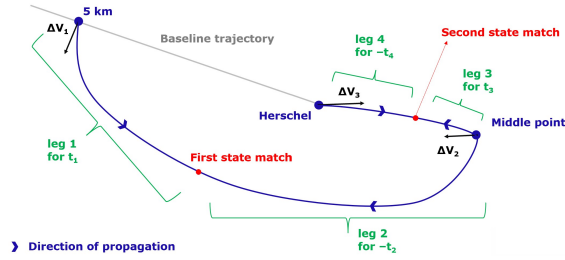
Fig. 9: Optimization Scheme

of the SO to rotate around two of its body axis. In order to avoid the Sun rays to hit the cryostat these rotations are bounded within $\pm 30°$ around the x body axis and $\pm 10°$ around the z body axis.

A flanking manoeuvre has been implemented to avoid reaching Herschel from the front, as the baseline trajectory identified in the previous chapter does. By doing this the cargo s/c approaches the SO from the back, where the docking port is located, and with a low relative velocity. A multiple shooting technique has been employed to perform this manoeuvre. The manoeuvre is implemented as an optimization problem following the scheme in figure 9.

The strategy makes use of three brakes: the first at the start at 5 km, the second at a point behind Herschel (middle point) and the last one at few meters from Herschel itself. The first one deviates the cargo from the baseline trajectory, allowing it to turn around Herschel, the second acts as a checkpoint and directs the cargo towards the observatory, the third aligns the chaser's velocity to the target's one, making the s/c almost still w.r.t. Herschel.

The propagation is performed in two directions, backward and forward, for each piece of trajectory between the impulses given. A total of four legs is obtained, that are constrained to match two by two.

5.1 *Optimization variables*
- 3 $\mathbf{\Delta V}_\mathrm{s}$ as vectors ($\mathbf{\Delta V}_1$, $\mathbf{\Delta V}_2$, $\mathbf{\Delta V}_3$) $\longrightarrow$ 9 variables;

- 4 times of flight (t_1, t_2, t_3, t_4) $\longrightarrow$ 4 variables;

- State of the middle point (x, y, z, $\dot{x}$, $\dot{y}$, $\dot{z}$) $\longrightarrow$ 6 variables.

In total there are 19 optimization variables.

5.2 *Constraints*
- State forward propagated from the starting point for t_1 seconds perturbed with $\mathbf{\Delta V}_1$ matches

the state backward propagated from the middle point for $- t_2$ seconds;

- State forward propagated from the middle point for t_3 seconds perturbed with $\mathbf{\Delta V}_2$ matches the state backward propagated from Herschel for $- t_4$ seconds perturbed with $\mathbf{\Delta V}_3$;

- $\Delta V_3 < 10$ m/s

In total there are 12 equality constraints on the matching of the states and 1 inequality constraint on the magnitude of the last impulse.

5.3 *Cost function*
The cost function for the optimization has been initially set to 1 to study the feasibility of the problem.

5.4 *Boundaries*
The middle point has been bounded in an ellipsoid of axes 2 x 1 x 1 km aligned to the synodic axes to maximize the probability that the last leg of approach occurs within the cone of approach. The times of flight have been bounded between 1 and 23 hours each, since employing less time than the former boundary or more than the latter boundary would result in a manoeuvre too fast or too slow respectively. The other variables have been left unbounded.

5.5 *Initial Conditions*
The initial conditions given are the following:

- $[0\ 0\ 0]^\mathrm{T}$ for the three $\mathbf{\Delta V}_\mathrm{s}$;

- The time of flight of the baseline trajectory to reach Herschel from the starting point for the four times (22.3 seconds);

- Herschel's state at rendezvous for the middle point.

5.6 *Results*
Among the different points studied on the Lissajous orbit, feasible solutions were obtained on the trajectory departing from a point on the right side of it, requiring 420 m/s of ΔV and a little bit more than 29 days of travel to reach the Moon. The manifold obtained is shown in figure 10, which contains some of the rendezvous trajectories that reach Herschel as imposed by the optimizer. In the figure only the solutions requiring from 6 to 10 hours have been displayed, but convergence of the simulator has been achieved for any time of flight between 1 and 23 hours.

This represents the asset of this manoeuvre, because in case the observatory isn't visible by the antennas of the Deep Space Network *(DSN)* to establish a connection, the departure from the Moon can be delayed hour after hour until this condition is satisfied. In short, there are multiple launch windows for this mission and since the Earth revolves around its axis in more or less 24 hours, the mission can start at any hour of the day.
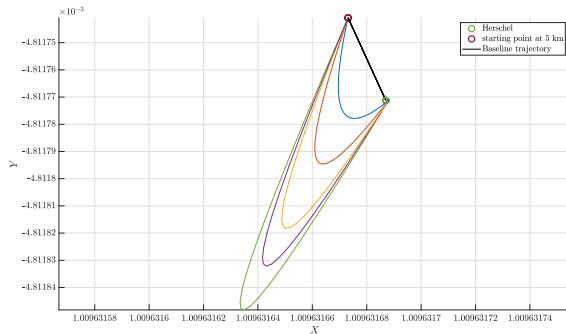

Fig. 10: Manifold of rendezvous trajectories lasting from 5 to 10 hours

For the rest of the paper the study has been focused on only one of these solutions, the one shown in figure 11. Table 2 contains the details of this manoeuvre in terms of magnitude of the impulses and times of flight.

Table 3 contains the errors from the desired point reached at the end of the rendezvous. The low velocity error makes the cargo spacecraft almost still w.r.t. Herschel so that the docking phase can be executed.

The only drawback of this solution is that the final leg of the approach is not restrained in the approach cone in the x-z plane, whereas no problems are encountered in the x-y plane, as the red rectangle in figure 11 shows.
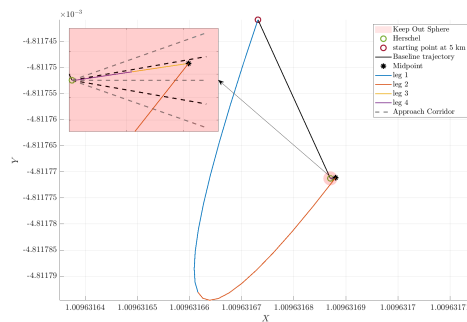

Fig. 11: Rendezvous phase

ΔV_1	331.3 m/s
ΔV_2	180.6 m/s
ΔV_3	$8.4 \cdot 10^{-2}$ m/s
ΔV_{TOT}	511.9 m/s
ToF	7 h 0 m 1 s

Table 2: Magnitude of the three impulses and total time of flight of the rendezvous phase

Position Error [mm]	Velocity Error [mm/s]
0.459	0.17

Table 3: Position and Velocity errors from the desired point

By using the Hill dynamics instead of the non-linear one similar results have been obtained. The main problem was constituted by the very high dependence on the initial conditions, since a small change brought to an unfeasible solution. Moreover, each leg of the trajectory needed at least 10 steps of resolution of the linear system in order to for the optimizer to converge. The upside is that the computational time is much lower, therefore the more optimization are performed the more is gained in time.

6. Attitude Control

The mission is at a first stage of development and the structure, systems and features of the cargo spacecraft are not completely defined yet. Many assumptions, then, have been made in order to obtain results for a simple control methodology, and it is for this reason that the model described below doesn't include sensor noises, but it assumes that the state computed by the kinematics and the dynamics after the application of the control torques is the one estimated by the sensors. Moreover, external disturbances are neglected for the following reasons:

- Atmospheric Drag is absent at SEL$_2$ because of its distance from Earth;

- Magnetic torques are excluded since the libration point is highly beyond the external Van Allen belt;

- The observatory revolves around an equilibrium point, meaning that the sum of all the gravity forces acting on the body is almost zero. This

implies that the torques exerted by these forces are negligible. A fast analysis of the GG torques points out that the magnitude of this disturbance is around 10^{-41} $N \cdot m$ for the x and y component, whereas the z component is around 10^{-60} $N \cdot m$.

- The Solar Radiation Pressure is the most important disturbance for this scenario, since the particles coming from the Sun reach very far distances and generate torques while hitting the spacecraft. In order to compute the magnitude of this disturbance however, some details of the structure of the cargo are needed, such as the material and its reflectivity. These data are not available yet, therefore, this disturbance is neglected as well.

The current available details of the cargo s/c are its body frame and its inertia matrix. The body frame has its origin at the cargo's centre of mass and three axes coincident with the three principal axes of inertia. It features the cryostat in the positive z direction and the main thruster opposite to it, whereas the camera is in the positive x direction. The inertia matrix provided is calculated in the body frame of the cargo in order to be considered constant.

6.1 _Dynamics & Kinematics_

The dynamics used involves Euler's equations:

$$\mathbb{J}^b \dot{\boldsymbol{\omega}}^b = -\boldsymbol{\omega}^b \times \mathbb{J}^b \boldsymbol{\omega}^b + \boldsymbol{M}_{app}^b \qquad (9)$$

where $\mathbb{J}^b$ is the aforementioned inertia matrix, $\boldsymbol{\omega}^b$ is the angular velocity vector, $\dot{\boldsymbol{\omega}}^b$ is the angular acceleration and $\boldsymbol{M}_{app}^b$ is the vector of the applied torques. Just as $\mathbb{J}^b$, all the variables are expressed in the body frame. Quaternions have been chosen as attitude parameterization, therefore the kinematics of a rigid body can be expressed as:

$$\dot{\mathfrak{q}}^{ib} = \frac{1}{2} \mathfrak{q}^{ib} \circ \boldsymbol{\omega}^b \qquad (10)$$

where $\mathfrak{q}^{ib}$ is the quaternion that rotates any vector expressed in the body frame to its inertial frame counterpart and $\dot{\mathfrak{q}}^{ib}$ is its time derivative.

6.2 _Controller_

The control technique employed is an error-quaternion feedback control [18], which allows the computation of the control torque needed to reach the desired attitude in absence of noise:

$$\boldsymbol{M}_{ctrl}^b = \boldsymbol{\omega}^b \times (\mathbb{J}^b \boldsymbol{\omega}^b) - \mathbb{K}_d \, \boldsymbol{\omega}_e - q_{e,0} \mathbb{K}_p \, \boldsymbol{q}_e \qquad (11)$$

where $\mathbb{K}_d$ and $\mathbb{K}_p$ are positive definite gain matrices, $q_{e,0}$ is the scalar part of the error unit quaternion and $\boldsymbol{q}_e$ is the vectorial one, and $\boldsymbol{\omega}_e$ is the error angular velocity vector. The error quaternion is defined as:

$$\mathfrak{q}_e = \tilde{\mathfrak{q}}_d \circ \mathfrak{q}^{ib}$$

where $\tilde{\mathfrak{q}}_d$ is the quaternion conjugate of the desired quaternion. On the other side, the error angular velocity is defined as:

$$\boldsymbol{\omega}_e = \boldsymbol{\omega}^b - \boldsymbol{\omega}_d$$

where $\boldsymbol{\omega}_d$ is the desired angular velocity that satisfies the kinematic constraints (11) and can be computed from the desired quaternion as $\boldsymbol{\omega}_d = 2\tilde{\mathfrak{q}}_d \circ \ddot{\mathfrak{q}}_d$.

6.3 _Actuator_

Since no actuation system has been chosen yet for the attitude control, monopropellant thrusters are assumed for this study [19], the same adopted by Herschel in the original mission for the same purpose. Four thrusters are dedicated to each axis, two per side, allowing a full attitude control around each axis. Figures 12 and 13 show the projections, on the x-y plane and y-z plane respectively, of the cargo spacecraft. The thrusters are located along the axes and positioned so that the exhaust doesn't hit the square platform where the camera is located. The signs + and - indicate the direction of the generated torque w.r.t. the body axes. This placement allows to have a net force equal to 0 so that the orbit is not perturbed and only the attitude is changed.
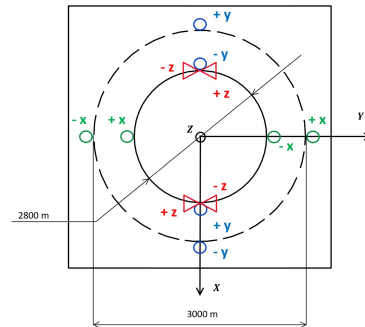

Fig. 12: Projection on the x-y body plane of the cargo spacecraft with the thrusters location

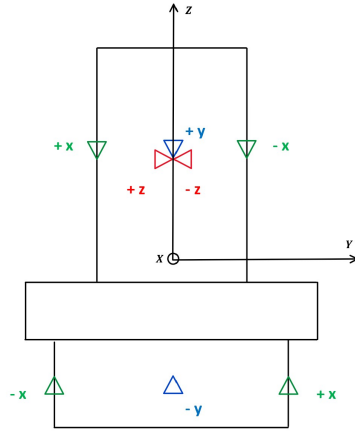In order to assure that these limits are not exceeded during the thrusts, a Schmidt Trigger _(ST)_

Fig. 13: Projection on the y-z body plane of the cargo spacecraft with the thrusters location

has been introduced. For single axis control, the system can be defined using two equations [20]:

$$\text{Minimum Pulse Width} = \frac{J\,h}{\tau\,T_c} \qquad (12)$$

$$\text{Limit Cycle Amplitude} = \frac{T_c\,(U_{on} + U_{off})}{2} + \frac{J^2\,h^2}{8\,\tau} \quad (13)$$

where h = $U_{on} - U_{off}$ and τ is the linear switching line slope, the tunable parameter dependent on the two gains K_p and K_d, which are scalar values for single axis control.

The first equation delivers the width h, after the minimum pulse width is obtained. This values is linked to the minimum impulse bit *(MIB)*, acquired from the data sheets of the thrusters, as MIB = $\Delta t \cdot T_c$, with Δt being the minimum pulse width. The parameter h is calculated considering the worst case scenario, meaning that J = J_z because it is the lowest value of the inertia matrix and is more affected by the dynamics, therefore it needs to be controlled more than the other axes. Consequently $T_c = T_{c,z}$. Once h is found, either U_{on} or U_{off} has to be chosen. The equation (13) links both of them to the limit cycle amplitude *(LCA)*, which becomes the second tunable parameter.

6.4 *Simulations*

The goal of the attitude control is double:

- Aligning the main cargo thruster to the direction of the $\mathbf{\Delta V}_s$ at each burn;

- Maximizing Herschel's visibility for the camera.

Knowing how the body frame of the cargo s/c is oriented, the first point implies that the negative z-axis of the cargo has to be aligned to the $\mathbf{\Delta V}$ vectors at 5 km, at the middle point and at the final point. The starting point at 5 km is set as initial condition, therefore the cargo is assumed to be already oriented correctly. The attitude control in this case consists only in a sequence of slew manoeuvres in which the cargo's attitude is changed during the trajectory to reach the final desired attitude at the burns, but without chasing any particular condition in between. The second condition implies that the positive x-axis points always to Herschel. In this case the attitude control consists in a tracking manoeuvre in which the desired attitude changes every instant while the cargo moves in space.

The slew manoeuvre by itself is executed smoothly in fact the controller takes less than 4 minutes to bring the angular error below 1°. For the rest of the manoeuvre, the error remains between 0.1° and 0.2°, except for the peak that represents the change of the desired quaternion after the burn at the middle point is executed. At that moment, the control system starts chasing the final attitude in which the negative z body axis is aligned to $\mathbf{\Delta V}_3$. The control is considerably fast if compared to the duration of the leg from the starting to the middle point, therefore, in case only the slew manoeuvre was to be performed, the control can be started few minutes before the middle point is reached in order not to waste fuel for nothing. The mass flow rate for a single thruster ranges between $\dot{m} = 3.2$ g/s and $\dot{m} = 10.4$ g/s. The average of this range is $\dot{m} = 6.8$ g/s, therefore, in case the control was performed for the entire RdV phase the total mass burnt would be 100 g of propellant. Instead, by choosing to activate the actuators 1500 seconds before it, the fuel consumption lowers to 24.6 g of propellant.

The tracking control is implemented only between the first two impulses because the time employed to go from the middle to the final point is too short and allows to execute only the slew manoeuvre. The error quaternion decreases to 0.28° very fast and stays below 0.3° for all the duration of the tracking manoeuvre. In this case the angular error goes to 360° which is the same as 0°. Normally this kind of controller would be too simple for a tracking problem, but the simulations proved that the slow changing rate of the quaternions enhanced the performance of this simple controller for this particular case and allowed it to perform well nonetheless. The mass of fuel consumed for the tracking manoeuvre is m = 24.3288
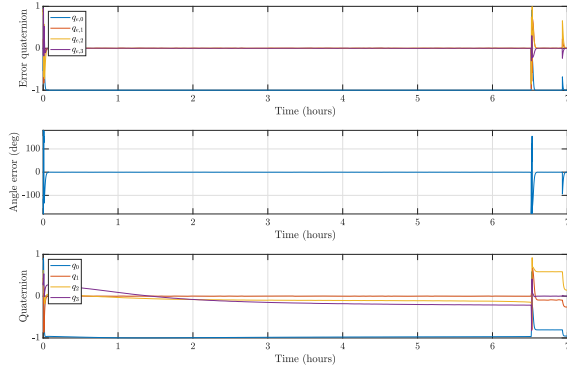
Fig. 14: Quaternion error, quaternions and angular error for the whole manoeuvre

Fig. 15: Peaks in the control torques needed to re - align the cargo S/C after the switch in the desired attitude

kg, much higher than the slew one. This result was expected since the spacecraft needs to be controlled all the time until the slew manoeuvre starts, which, in fact, represents only the 7 % of all the RdV phase. The complete manoeuvre, involving both the slew and the tracking phase is executed as follows: starting from the 5 km of distance from Herschel, tracking starts, in order to align the camera towards Herschel. This attitude is maintained during most of the trajectory until the cargo s/c is close to the middle point. 1500 seconds before reaching it, the desired quaternion switches to the direction of $\boldsymbol{\Delta V}_2$ and the first slew manoeuvre starts. After the burn is executed, the second slew manoeuvre starts in order to align the main thruster to the direction of $\boldsymbol{\Delta V}_3$, where the control ends. Figure 14 shows the variation of the quaternion error, quaternions and angular error for the whole simulation. It can be seen that, when the desired attitude is changed to start the two slew manoeuvres, there is a peak, but they are soon flattened by the control system that brings the error close to 0 again.

Figure 15 shows the control command as well as the applied torques, pointing out how the high torque necessary to align the chaser to the desired attitude is spread all over the rendezvous phase. The figure also depicts the two peaks in the control torques that the control system generates at the switch from one desired attitude to the other. Therefore, the first one represent the switch from tracking to slew 1 and the second from slew 1 to slew 2.

The fuel needed in case both the manoeuvres are performed is m = 24.3652 kg, where the fuel consumed for the tracking manoeuvre is 99 % of the total, the 24.3288 kg seen before. The remaining 36.4 g are used for the slew manoeuvres in the last part of the RdV phase.
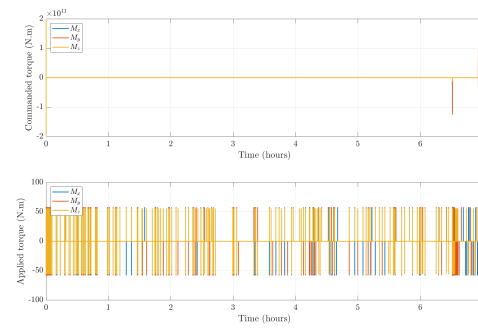
The results obtained could be changed according to the needs of the mission. If the main objective is minimizing the mass on board, the tunable parameters of the ST can be changed so that the thrusters would activate less times during the manoeuvre, ending up with a higher final angular error, but gaining in quantity of fuel consumed.

The attitude control is independent of the orbit described by the chaser during the rendezvous phase. This is mainly due by the absence of perturbation in the model used. Therefore, each one of the manoeuvres computed in the previous chapter, lasting different times, can be controlled in the same way this one was. Clearly, those taking less time will have a lower fuel consumption that those employing more hours to reach Herschel. By taking into account the departure time from the Moon, the time of flight of the RdV phase and the transportable mass on board, the final path for the HRSM mission can be determined.

7. Conclusion

The paper addresses the problem of on-orbit servicing in the 3-body problem, presenting a re-supply mission for the Herschel Space Observatory, orbiting around the Sun-Earth L_2 point. This work presents a preliminary trajectory design to find a manifold of trajectories that link the Moon, the departure point of the mission, with Herschel. These trajectories have been obtained by backward propagating Herschel's state on the Lissajous orbit perturbed by an impulse. The grid search allowed finding the ΔV that needs to be added to Herschel's velocity in order to reach the Moon. The equations of motion have been simplified using two different methodologies, compared to the non-linear equations and to one another, in order to

find a set of equation that can be used to speed up the simulations without adding too many errors to the computation. A rendezvous manoeuvre has been implemented adopting multiple shooting technique to approach Herschel from the rear side, where the docking port is located. The manoeuvre allowed the cargo s/c to reach Herschel and stop at only 2 meters from it with almost null relative velocities, but with an approach that occurred out of the cone of approach in the x-z plane. Nevertheless this method has the advantage of having solutions employing different times of flight to approach Herschel, from 1 to 23 hours, so that the mission can start any time during the day with the assurance of having full coverage by the antennas of the DSN. Finally the paper presents a simplified model for the attitude control, exploiting an error-quaternion feedback control law to perform a slew and a tracking manoeuvre so that the two constraints of this part of the mission are met: main engine in the direction of the thrusts and camera always pointing at Herschel. The performance of this controller have been evaluated and the fuel needed for the manoeuvre has been computed. Future works foresee a better adaptation of the final approach to align with the corridor for docking. Furthermore, the spacecraft will be provided with robotic arms for the clamping sequence during docking operations, therefore the attitude control will be adapted to compensate for the angular rates induced by the movements of these robotic arms.

Acknowledgment

References

[1] Andrea Siena. Orbit/attitude control for rendezvous & docking at the herschel space observatory, 2021-2022.

[2] JR Burton and WE Hayes. Gemini rendezvous. *Journal of Spacecraft and Rockets*, 3(1):145–147, 1966.

[3] Manny R Leinz, Chih-Tsai Chen, Peter Scott, William Gaumer, Peter Sabasteanski, and Michael Beaven. Modeling, simulation, testing, and verification of the orbital express autonomous rendezvous and capture sensor system (arcss). In *Sensors and Systems for Space Applications II*, volume 6958, page 69580C. International Society for Optics and Photonics, 2008.

[4] Thomas V Peters, João Branco, Diego Escorial, Lorenzo Tarabini Castellani, and Alex Cropp. Mission analysis for proba-3 nominal operations. *Acta Astronautica*, 102:296–310, 2014.

[5] Simone D'Amico, J-S Ardaens, Gabriella Gaias, Heike Benninghoff, Benjamin Schlepp, and JL Jørgensen. Noncooperative rendezvous using angles-only optical navigation: system design and flight results. *Journal of Guidance, Control, and Dynamics*, 36(6):1576–1595, 2013.

[6] Jean-Sébastien Ardaens and Gabriella Gaias. Angles-only relative orbit determination in low earth orbit. *Advances in Space Research*, 61(11):2740–2760, 2018.

[7] Jean-Sébastien Ardaens and Gabriella Gaias. Flight demonstration of spaceborne real-time angles-only navigation to a noncooperative target in low earth orbit. *Acta Astronautica*, 153:367–382, 2018.

[8] Gabriella Gaias and Jean-Sébastien Ardaens. Flight demonstration of autonomous noncooperative rendezvous in low earth orbit. *Journal of Guidance, Control, and Dynamics*, 41(6):1337–1354, 2018.

[9] JM Rebordão. Space optical navigation techniques: an overview. In *8th Iberoamerican Optics Meeting and 11th Latin American Meeting on Optics, Lasers, and Applications*, volume 8785, page 87850J. International Society for Optics and Photonics, 2013.

[10] Josep Virgili Llop. Autonomous optical navigation for orbits around earth–moon collinear libration points. *Acta Astronautica*, 86:119–125, 2013.

[11] David Folta, Steven Cooley, Kathleen Howell, and Frank H Bauer. Trajectory design strategies for the ngst l2 libration point mission. In *Space Flight Mechanics*, 2001.

[12] Salman Ali Thepdawala. Preliminary trajectory design for cis-lunar libration point mission. In *International Conference of Control, Dynamic Systems, and Robotics*. Avestia Publishing, may 2021.

[13] David C Folta and Cassandra Webster. Transfer trajectory options for servicing sun-earth-moon libration point missions. In *Proc. 29th AAS/A-IAA Space Flight Mech. Meeting*, 2019.

[14] Victory Szebehely. *Theory of orbit: The restricted problem of three Bodies*. Elsevier, 2012.

[15] ESA. Herschel, 2021.

[16] Martin Hechler and Jordi Cobos. Herschel, planck and gaia orbit design. In *Libration Point Orbits and Applications*, pages 115–135. World Scientific, 2003.

[17] GL Pilbratt, JR Riedinger, T Passvogel, G Crone, D Doyle, U Gageur, AM Heras, C Jewell, L Metcalfe, S Ott, et al. Herschel space observatory-an esa facility for far-infrared and submillimetre astronomy. *Astronomy & Astrophysics*, 518:L1, 2010.

[18] Ahmed Mahfouz, Dmitry Pritykin, and James Biggs. Hybrid attitude control for nano-spacecraft: Reaction wheel failure and singularity handling. *Journal of Guidance, Control, and Dynamics*, 44(3):548–558, 2021.

[19] ArianeGroup. 20N hydrazine thruster. https://www.space-propulsion.com/spacecraft-propulsion/hydrazine-thrusters/20n-hydrazine-thruster.html. Accessed: 2022-02-17.

[20] Bong Wie. *Space Vehicle Guidance, Control and Astrodynamics*. American Institute of Aeronautics and Astronautics, Inc., 2015.